Ultrasound-modulated optical imaging using a high-power pulsed laser and a double-pass confocal Fabry-Perot interferometer

Rousseau, Guy; Blouin, Alain; Monchalin, Jean-Pierre

Publisher's version / Version de l'éditeur:
https://doi.org/10.1364/OL.34.003445
Optics Letters, 34, 21, pp. 3445-3447, 2009-11-01

Ultrasound-modulated optical imaging using a high-power pulsed laser and a double-pass confocal Fabry-Perot interferometer

Guy Rousseau,* Alain Blouin, and Jean-Pierre Monchalin

Industrial Materials Institute, National Research Council of Canada

75 de Mortagne Blvd., Boucherville, Québec, Canada, J4B 6Y4

**Corresponding author: guy.rousseau@cnrc-nrc.gc.ca*

We report the use of short ultrasonic bursts and high-peak-power laser pulses to detect absorbing objects in thick scattering media. The detection of ultrasound-tagged photons is performed with a double-pass confocal Fabry-Perot interferometer. Photons shifted by the fundamental and harmonic frequencies of the ultrasonic bursts were observed. Absorbing objects were detected in 30- and 60-mm thick scattering media including a biological tissue sample.

OCIS codes: 170.1065, 170.3880, 170.7050, 300.6320.

Optical imaging techniques for biomedical diagnostics are currently actively developed. These techniques are based on non-ionizing radiation and provide morphological as well as functional information. Ultrasound-modulated optical imaging (or tomography) allows the localization of absorbing or scattering objects embedded in optically scattering media through the detection of ultrasound-tagged photons [1-8]. This method combines the mm-scale spatial resolution and the cm-scale penetration depth of ultrasonic waves with the spectroscopic information provided by

light. A practical limit is the poor sensitivity or low signal-to-noise ratio of the technique. Moreover, for biomedical applications, safety considerations limit the power level of the ultrasonic wave and the laser beam [9-10].

The use of a confocal Fabry-Perot interferometer (CFPI) as a spectral filter has already been implemented for the detection of ultrasound-tagged photons [1]. With a CFPI, the detection of a faint spectral line (tagged photons) close to a strong one (untagged photons) can be difficult when the rejection of the latter is to low. However, the rejection can be significantly improved by cascading multiple CFPI or by using a multipass configuration [11-12]. Although renowned for its large optical etendue compared to other spectrometric devices [13], the CFPI remains the limiting component of the setup in terms of optical gathering power. This can be in part overcome by maximizing the optical illumination of the scattering medium with high-peak-power single-frequency laser pulses [4]. When compared to photorefractive detection [2-4] and spectral hole burning [8], the CFPI can be easily implemented at any wavelength in the therapeutic window. Moreover, the response time of the CFPI is almost instantaneous (sub-μs) when compared to the *in vivo* speckle decorrelation time (ms range).

In our experiment, a double-pass CFPI was used for the detection of photons tagged by a frequency shift equal to the ultrasound frequency or its harmonics. The experimental setup is schematically shown in Fig. 1(a). The single-frequency laser pulses (1.064-μm wavelength) emitted by a Nd:YAG master oscillator power amplifier (MOPA) illuminate the cell containing the scattering medium (SM). The layout of the MOPA was described in a previous publication [4]. The SM is insonified with a focused ultrasonic transducer (UT: 19-mm diameter, 45-mm focal length) fed with 10-cycle bursts at 5 MHz. At the back face of the SM, photons are injected in a multimode optical fiber (MF: core diameter ϕ = 1 mm, numerical aperture NA = 0.36,

etendue $U_{MF} = (\pi \phi NA / 2)^2 = 0.32$ mm^{2}sr) and sent toward the double-pass CFPI. The signal beam at the output the MF is collimated with a lens, polarized by a polarizing beamsplitter (PBS) and coupled to the CFPI for a first pass. The CFPI is characterized by a free spectral range FSR = 75 MHz (cavity length L = 1 m) and a finesse $F = \pi R / (1-R^2) = 28$ (mirrors reflectivity R = 94.5%). The beam exiting the CFPI is reflected back by a plane mirror (PM) and the polarization is rotated by 90° with a quarter-wave plate (QW). After the second pass, the beam is redirected by the PBS toward an InGaAs-PIN photodiode (PD: 0.5-mm diameter, 400-kHz bandwidth). The finite optical etendue of the CFPI, $U_{CFPI} = \pi^2 L \lambda / F = 0.38$ mm^{2}sr, is obtained for an effective single-pass finesse $F_1 \equiv 0.7$ F [13]. The intensity transmission function of the double-pass configuration is equal to the square of the single-pass transmission function which results in an effective double-pass finesse $F_2 = 1.6$ F_1. Consequently, in the double-pass configuration, the CFPI was equivalent to a tunable bandpass filter with a full-width-at-half-maximum (FWHM) equal to FSR / F_2 = 2.4 MHz. This value was larger than the FWHM of the ultrasonic burst power spectrum (0.5 MHz) and sufficiently narrow to reject the untagged photons by about 18 dB when the peak transmission of the CFPI was tuned at 5 MHz from the laser frequency. Figure 1(b) presents a typical laser pulse intensity profile. A peak power of more than 1 kW was routinely obtained at a repetition rate of 25 Hz. The pulse duration was adjustable and typically set to a FWHM of 90 μs to get a plateau of constant optical power. In clinical applications, the optical illumination of the SM could be limited to the time of flight of the ultrasonic burst in the focal zone (20 μs). Consequently, the value of average irradiance mentioned hereafter was calculated by considering a laser pulse duration of 20 μs. By illuminating the SM with a 30-mm diameter laser beam, the average irradiance was equal to 90 mW/cm^2, which is well below the safety limit (1 W/cm^2 at 1.064 μm) [10]. Figure 1(c) presents the lateral profile of pressure in the

transducer focal plane when the UT was fed by the maximum driving voltage. This profile was measured with a heterodyne interferometer as described in ref. [4]. The peak pressure of 1.9 MPa was below the safety limit at 5 MHz (4.2 MPa) [9].

The first measurements were performed on a 30-mm thick SM composed of TiO_2 particles (DuPont Ti-PURE R-900, medium particle size: 0.41 μm) dispersed in sunflower oil with a concentration giving a scattering mean-free-path l_s = 170 μm. Figure 2 shows the tagged-photon signal as a function of the ultrasonic pressure at focus. The data points correspond to tagged photons shifted by 5 (circles), 10 (triangles), and 15 MHz (squares). A quadratic fit with the 5-MHz signal at pressures below 1 MPa is also shown. It is clearly seen that, at higher ultrasonic pressures, the second harmonic of the ultrasound frequency is no more negligible and is responsible of the departure of the 5-MHz signal from the quadratic law. The vertical zoom in Fig. 2(b) shows the onset of the second and third harmonic signals. It thus appears that the effective modulation depth induced by the pressure wave is sufficiently large to generate multiple optical sidebands [14]. Photons tagged by the fundamental ultrasound frequency were used to obtain the following results.

Images of embedded objects were obtained from a temporal to spatial mapping for the ultrasound propagation axis z (the speed of sound is approximately equal to 1.5 mm/μs) as a function of the lateral position x of the transducer. Figure 3 shows the image of a piece of jellified India ink (3x3x3 mm^3) suspended in the central plane of the 30-mm thick SM. The signal-to-noise ratio of this image is acceptable considering that it was obtained without averaging. Horizontal and vertical profiles passing through the center of the object are respectively shown on the top and right-hand side of the image. Figure 4 compares images obtained with (left) a 3x3x3 mm^3 piece of jellified India ink and (right) with a 4x5x5 mm^3 piece

of white putty which is a strong ultrasound absorber. Both images were obtained with 16-line averaging (average of 16 signals for each vertical line). By comparing the horizontal profiles on top of both images, it is clearly seen that the edges sharpness (the slope of the signal at each edge) is lower in the vicinity of the optically absorbing object (left). The degradation of the edges sharpness of an optically absorbing object can be attributed to the diffuse propagation of the photons tagged in its vicinity. Indeed, these tagged photons, by following non-ballistic paths are more likely to be absorbed by the object before exiting its neighborhood. In ultrasound-modulated optical imaging, this effect may lead to a lower image sharpness than what would be expected from the ultrasound beam diameter and burst duration. However, this effect may also be used to evaluate the scattering properties of the medium surrounding the object. Figure 5 shows the image (256-line average) of a piece of jellified India ink (3x3x3 mm^3) located in the central plane of a 60-mm thick SM. Again, the horizontal profile on the top of the image clearly shows that the width of the step corresponding to each edge of the object is wider than the width that would be expected from the diameter of the ultrasound beam (see Fig. 1(c)), thus confirming the previously mentioned tendency.

In applications involving biological tissues, the attenuation will limit the penetration depth of ultrasound. For probing a 60-mm thick sample of chicken breast, we have used a 2.25-MHz focused UT (38-mm diameter, 51-mm focal length) fed with 5-cycle bursts. The ultrasonic beam was first characterized in water and its diameter (FWHM of the intensity profile) was measured to be equal to 0.9 mm in the focal plane. The detection of a piece of jellified India ink (3x3x3 mm^3) located in the central plane of the 60-mm thick sample of chicken breast was performed with the optical illumination described previously. The peak pressure in the focal plane of the transducer was equal to the safety limit at 2.25 MHz (2.9 MPa) by assuming an

ultrasonic attenuation of 2 dB/cm in the chicken breast sample. This value of the attenuation was measured with two transducers in transmission mode. When using 2.25-MHz bursts, the peak transmission of the CFPI was tuned at about 3.4 MHz from the laser frequency to obtain an optimal visibility of the tagged photons while maintaining an acceptable rejection of the untagged photons. The image (128-line average) of the object is shown in Fig. 6. To our knowledge, this is the first image obtained in such a thick biological tissue by using ultrasound-modulated optical imaging.

In summary, we have shown that the detection of photons tagged by low-frequency ultrasonic bursts can be performed with a double-pass CFPI. The limited optical etendue of the CFPI has been compensated by the use of high-power single-frequency laser pulses. The optical etendue and the rejection of the untagged photons could be both increased by using a longer CFPI. Photons shifted by harmonics of the ultrasound frequency were observed and are not negligible even for peak pressures below the safety limit. Absorbing objects were detected without averaging in a 30-mm thick SM. With averaging, it has been possible to probe a 60-mm thick sample of biological tissue. Such a result shows the good potential of the double-pass CFPI when combined with a pulsed laser source. The CFPI will also be easily implemented at any wavelength in the therapeutic window.

Guy Rousseau's e-mail address is guy.rousseau@cnrc-nrc.gc.ca.

References

1. S. Sakadžić and L. V. Wang, "High-resolution ultrasound-modulated optical tomography in biological tissues," Opt. Lett. **29**, 2770-2772 (2004).

2. T. W. Murray, L. Sui, G. Maguluri, R. A. Roy, A. Nieva, F. Blonigen, and C. A. DiMarzio, "Detection of ultrasound-modulated photons in diffuse media using the photorefractive effect," Opt. Lett. **29**, 2509-2511 (2004).

3. F. Ramaz, B. C. Forget, M. Atlan, A. C. Boccara, M. Gross, P. Delaye, and G. Roosen, "Photorefractive detection of tagged photons in ultrasound modulated optical tomography of thick biological tissues," Opt. Express **12**, 5469-5474 (2004).

4. G. Rousseau, A. Blouin, and J.-P. Monchalin, "Ultrasound-modulated optical imaging using a powerful long pulse laser," Opt. Express **16**, 12577-12590 (2008).

5. S. Lévêque, A. C. Boccara, M. Lebec, and H. Saint-Jalmes, "Ultrasonic tagging of photon paths in scattering media - Parallel speckle modulation processing," Opt. Lett. **24**, 181-183 (1999).

6. M. Atlan, B. C. Forget, F. Ramaz, A. C. Boccara, and M. Gross, "Pulsed acousto-optic imaging in dynamic scattering media with heterodyne parallel speckle detection," Opt. Lett. **30**, 1360-1362 (2005).

7. S.-R. Kothapalli, S. Sakadžić, C. Kim, and L. V. Wang, "Imaging optically scattering objects with ultrasound-modulated optical tomography," Opt. Lett. **32**, 2351–2353 (2007).

8. Y. Li, H. Zhang, C. Kim, K. H. Wagner, P. Hemmer, and L. V. Wang, "Pulsed ultrasound-modulated optical tomography using spectral hole-burning as a narrowband spectral filter," Appl. Phys. Lett. **93**, 011111 (2008).

9. F. A. Duck, "Medical and non-medical protection standards for ultrasound and infrasound," Prog. Biophys. Mol. Biol. **93**, 176-191 (2007).

10. Laser Institute of America, American National Standard for the Safe Use of Lasers ANSI Z136.1-2000 (ANSI, Orlando, Florida, 2000).

11. J. R. Sandercock, "Brillouin scattering study of SbSI using a double-passed, stabilised scanning interferometer," Opt. Commun. **2**, 73–76 (1970).

12. D. S. Cannell, J. H. Lunacek, and S. B. Dubin, "A simple double-pass spherical Fabry-Perot interferometer," Rev. Sci. Instrum. **44**, 1651–1653 (1973).

13. M. Hercher, "The Spherical Mirror Fabry-Perot Interferometer," Appl. Opt. **7**, 951-963 (1968).

14. J. Selb, L. Pottier, and A. C. Boccara, "Nonlinear effects in acousto-optic imaging," Opt. Lett. **27**, 918–920 (2002).

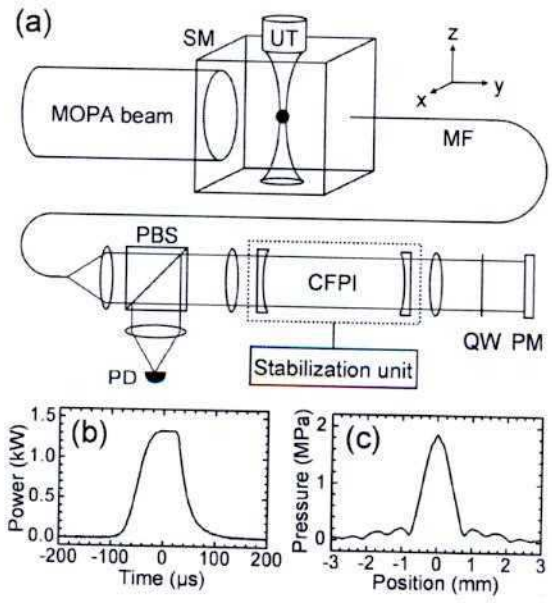

Fig. 1. (a) Layout of the setup. Abbreviations are defined in the text. Other components are lenses. (b) Pulse intensity profile at the exit of the MOPA. (c) Lateral distribution of the pressure wave in the focal plane.

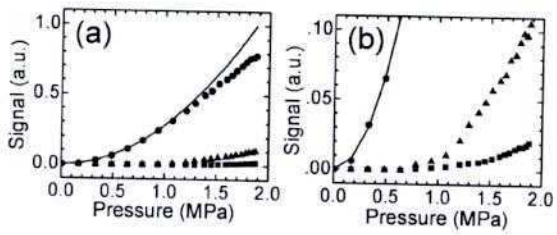

Fig. 2. (a) Tagged-photon signal at 5 (circles), 10 (triangles), and 15 MHz (squares). Solid line: quadratic fit. (b) Zoom of (a).

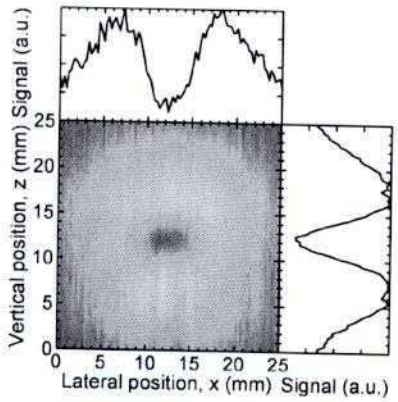

Fig. 3. (Color online) Image (without averaging) of a piece of jellified India ink (3x3x3 mm^3) in the central plane of a 30-mm thick SM.

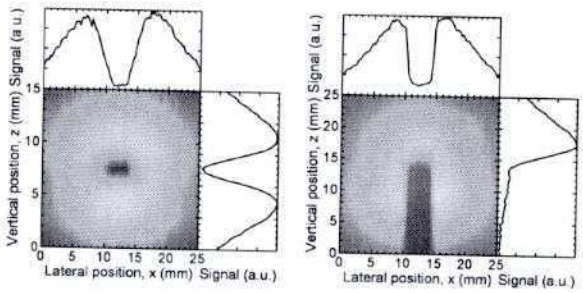

Fig. 4. (Color online) Images (16-line average) of objects in the central plane of a 30-mm thick SM. Left: piece of jellified India ink (3x3x3 mm^3). Right: piece of white putty (4x5x5 mm^3).

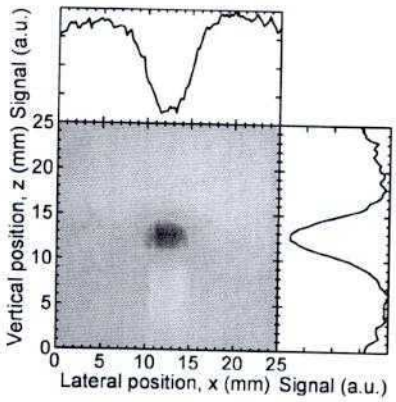

Fig. 5. (Color online) Image (256-line average) of a piece of jellified India ink (3x3x3 mm^3) in the central plane of a 60-mm thick SM.

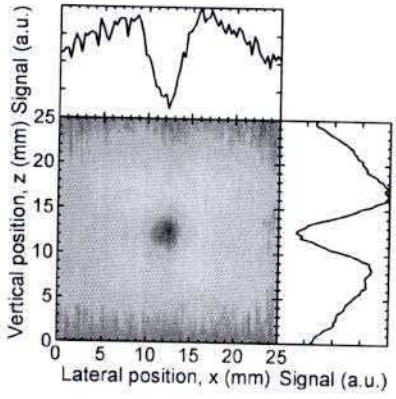

Fig. 6. (Color online) Image (128-line average) of a piece of jellified India ink (3x3x3 mm^3) in the central plane of a 60-mm thick sample of chicken breast.